Ore Geology Reviews 92 (2018) 257–270

Contents lists available at ScienceDirect

Ore Geology Reviews

journal homepage: www.elsevier.com/locate/oregeorev

Deciphering the tectonic-geodynamic context of the gem-quality "*noble serpentine*" deposit formation combining microstructural, chemical and micro-Raman analyses in Palaeozoic olivine-bearing marbles and serpentine-hosting rocks (Pizzo Tremogge, Margna unit – Austroalpine, Val Malenco – Central Alps, Italy)

Michele Zucali[a,*], Nicoletta Marinoni[a,b], Valeria Diella[b], Alessandro Croce[c], Caterina Rinaudo[c], Emanuele Fontana[a]

[a] Department of Earth Sciences "Ardito Desio", University of Milan, Via Botticelli 23, 20133 Milan, Italy
[b] National Research Council, IDPA, Section of Milan, Via Botticelli 23, 20133 Milan, Italy
[c] Department of Science and Technological Innovation, University of Eastern Piedmont, Viale Michel 11, 15121 Alessandria, Italy

ARTICLE INFO

Keywords:
Noble serpentine
Palaeozoic marbles
Val Malenco
Micro-Raman spectroscopy
Electron Microprobe Spectrometry
X-ray powder diffraction

ABSTRACT

The gem-quality "*noble serpentine*" of Pizzo Tremogge (Val Malenco, Italy) is included in Palaeozoic olivine-bearing marbles, occurring in the Margna unit, Central Austroalpine domain. A detailed inspection of serpentine samples reveals the presence of the three serpentine species (lizardite, chrysotile and antigorite) occurring in different microstructural domains.

Serpentine samples were investigated to obtain microstructural information preserved in the serpentine species by optical microscopy, X-ray powder diffraction, Electron Microprobe Spectrometry and Micro-Raman spectroscopy, the last of which is considered a reliable method for the identification of the different serpentine species.

Two types of "*noble serpentine*" have been identified: the yellow-green type characterized by fine-grained aggregates in marbles and the green type localized in fibrous veins in association with calcite and quartz.

The identification of the different serpentine types allowed us to recognize three stages of mineral crystallization characterized by: i) the formation of olivine-bearing marbles (Stage 1), ii) the growth of lizardite after olivine or within lizardite-rich veins (Stage 2) and iii) the replacement of lizardite by antigorite in marbles and by antigorite + clinohumite in veins (Stage 3).

These stages clarify the complex geodynamic-tectonic evolution of the Margna-Malenco system. The Paleozoic olivine-bearing marbles (Margna protoliths, Stage 1) are subjected to extensional tectonics that brings the Margna protoliths close to the Malenco in a thinned-extended-type passive margin (Stage 2). Finally, an inversion of tectonics leads to the subduction and collision of the Margna-Malenco system during alpine convergence (Stage 3). All this suggests that gem-quality "*noble serpentine*" deposits may be related to different geological contexts.

1. Introduction

Deposits of the gem-quality "*noble serpentine*", have been described worldwide associated with serpentinite or serpentinite-marble. Serpentinite rocks are observed in various tectonic settings and are common in various metamorphic and geodynamic contexts: from blueschist to eclogite facies conditions during subduction and exhumation, as well as in hydrothermal conditions during lithospheric extension due to the oceanic hydration and to alteration of olivine and magnesium-rich silicates from seawater (Evans, 2004; Evans et al., 2013; Mével, 2003). Recent works have also proposed a subduction-collision geodynamic context for the formation of "*noble serpentine*"-rich serpentinite deposits in the Urals (Posukhova et al., 2012, 2013).

Serpentinites are chiefly composed of the serpentine-mineral group, which includes hydrous magnesium phyllosilicates with an ideal chemical formula $Mg_3Si_2O_5(OH)_4$. From a crystallographic point of view,

* Corresponding author.
E-mail address: michele.zucali@unimi.it (M. Zucali).

https://doi.org/10.1016/j.oregeorev.2017.11.020
Received 24 May 2017; Received in revised form 15 November 2017; Accepted 22 November 2017
Available online 23 November 2017
0169-1368/ © 2017 Elsevier B.V. All rights reserved.

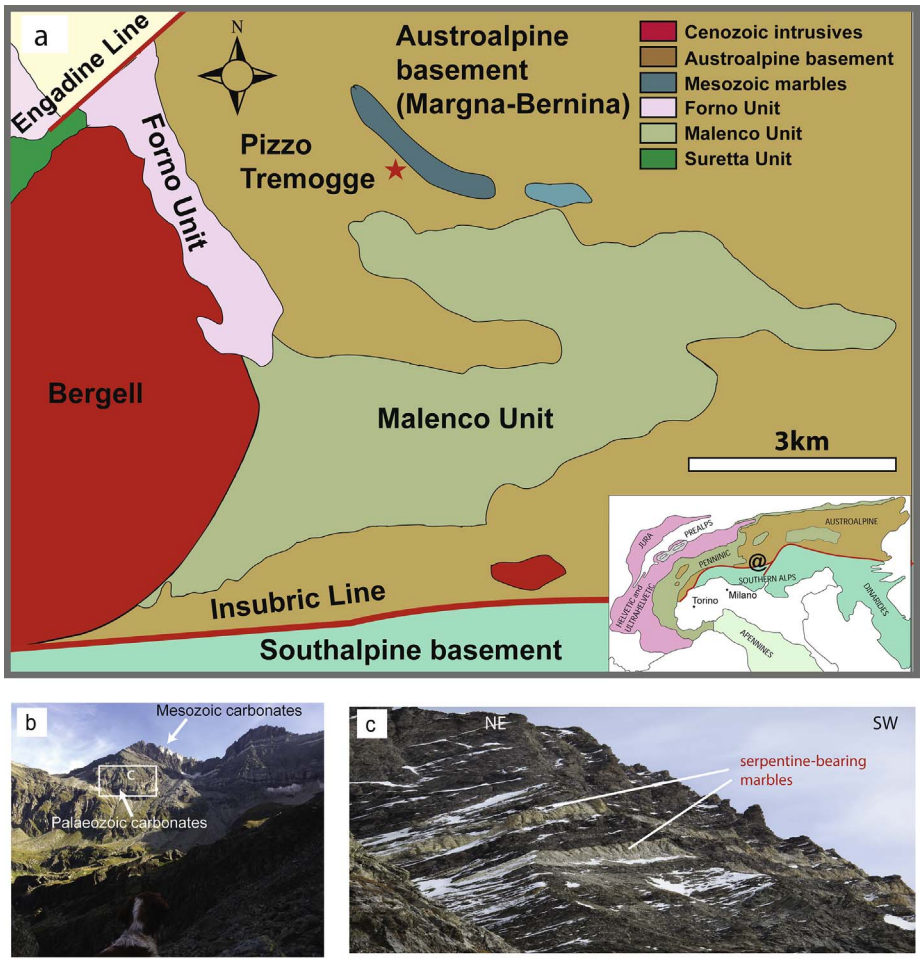

Fig. 1. (a) Schematic Geological map of Val Malenco, Italy, at 1:125.000 scale, showing the Margna Unit and Australpine basement (light brown) with Mesozoic cover (dark blue), the Malenco Unit (light green), the Forno Unit (pink), the Southern Alps (light blue) and the Cenzoic intrusives of Bergell and Triangia (dark red). The Insubric and Engadine lines are also reported (modified after Adamo et al., 2009); (b) Palaeozoic and Mesozoic marbles cropping out at Pizzo Tremogge; (c) Palaeozoic serpentine-bearing marbles cropping out at Pizzo Tremogge pass. Panoramic view of the relations between marbles (white), amphibolites (dark brown) and paragneisses (not visible in figure). (For interpretation of the references to colour in this figure legend, the reader is referred to the web version of this article.)

serpentines consist of superposed 1:1 alternating tetrahedral [SiO_4] and octahedral $Mg(O, OH)_6$ sheets and the different spatial arrangements of these layers result in three main structural varieties: the sheet form flat layers in lizardite, coiled cylinders in chrysotile and wavy structures in antigorite (Dodony et al., 2002; Laurora et al., 2011; Rinaudo et al., 2003; Wicks and O'Hanley, 1988).

The serpentines are schematically considered as pseudo-polymorphs even if important chemical differences exist, mainly due to the variable extent of the cationic substitutions in the structural sites (Viti and Mellini, 1997). The relative stability of each variety covers a wide range of metamorphic conditions: antigorite occurs under high-pressure and high-temperature conditions whereas lizardite and chrysotile are present in low-grade metamorphic rocks (Bromiley and Pawley, 2003; Hilairet et al., 2006; Padrón-Navarta et al., 2013; Ulmer and Trommsdorff, 1995, 1999; Wunder and Schreyer, 1997). Therefore, it is generally difficult to evaluate the P-T conditions under which serpentine minerals were subjected. Nevertheless, in the case of a well-constrained sampling area, the associated metamorphic rocks and related mineral parageneses allow an approximate knowledge of these conditions (Schwartz et al., 2013).

In this light, the correct identification of the serpentine varieties may be useful in providing fundamental data for evaluating the P-T conditions of metamorphic processes. Several analytical techniques have been used to identify serpentine minerals and to distinguish among them on the basis of their structural and chemical properties. Optical microscopy does not appear to be a valuable technique for their characterization because they have similar optical properties and are frequently fine grained and sub-microscopically intergrown. Transmission Electron Microscopy with EDS is the most reliable technique for serpentine identification but the sample preparation is difficult and time consuming and the interpretation of the electron diffraction pattern is not easy (Andreani et al., 2004, 2008). Wicks and O'Hanley (1988) reported that X-ray Diffraction was successfully used to distinguish among the three varieties. Rinaudo et al. (2003) proved that Micro-Raman Spectrometry is the most useful micro-characterization tool for resolving serpentine structural differences at the scale of the various grain generations. For instance, Groppo et al. (2006) investigated the serpentinite from the Lanzo Ultramafic Complex and demonstrated that micro-Raman allows a reliable identification of lizardite, antigorite and chrysotile, even when they are microscopically intergrown or form aggregates with other minerals. In Schwartz et al. (2013) Micro-Raman and Electron Microprobe Spectrometry (WDS) analyses combined with petrological observations of serpentine-bearing samples in the Western Alps gave useful insight into the estimation of the relative stability of each variety of serpentine and into the relationships of their distribution with the thermal evolution of the host-rock.

In the Central Alps a deposit of gem-quality serpentine, often referred to as "*noble serpentine*", occurs at Pizzo Tremogge, Val Malenco (Italy) and is included in Palaeozoic olivine-bearing marbles in the Margna unit (Central Austroalpine domain). Due to the compact microstructure and fine and green colour "*noble serpentine*" is used as gems and for ornamental carvings. Bedogné et al. (1993) and Benetti (1984) highlighted that the Pizzo Tremogge "*noble serpentine*" consisted of lizardite associated with white veins of calcite whereas Adamo et al. (2014, 2016) pointed out the simultaneous presence of lizardite, chrysotile and antigorite.

The geological and structural geodynamic context in which the

Pizzo Tremogge "*noble serpentine*" forms is still poorly understood. From lithological and structural observations, it has been interpreted as the result of the juxtaposition of the Austroalpine or continent-derived Margna unit to the ophiolite or oceanic-derived Malenco unit during the pre-Alpine extensional tectonics (Hermann et al., 1997). To our knowledge, there is no mineralogical and chemical data to validate that hypothesis.

In this view, the aim of the present study is to perform a detailed characterization of the "*noble serpentine*" (hereinafter referred to as serpentine) and its bearing rocks at the Pizzo Tremogge. Petrographic observations coupled with X-ray Powder Diffraction have allowed the identification of the mineralogical assemblage and microstructure of the serpentine bearing rocks. Furthermore, Electron Microprobe Spectrometry (WDS) and Micro-Raman spectroscopy were used to discriminate the different pseudo-polymorphs belonging to the serpentine minerals. The correct identification of the serpentine species provided us a useful support in understanding the microstructural relationships and in evaluating the structural and metamorphic processes of host rock and serpentine, as well as in proposing a simplified model for the evolution of serpentine-host rock, from pre-Alpine to Alpine age.

2. Geological setting

Samples were collected in the Margna unit (Fig. 1a, Pizzo Tremogge), central Austroalpine domain, constituted by the pre-alpine Palaeozoic continental crust involved in the Alpine subduction-collision system. It crops out close to the Forno and Malenco units, a fragment of oceanic mantle-derived rocks and ophiolites. The Margna basement is constituted by a pre-Permian association of metapelites with amphibolite to granulite metamorphic imprint, producing paragneisses and acid granulites associated with Ca-silicates and olivine-bearing calcitic marbles (Figs. 1b and c) and amphibolites. Late Variscan intrusive bodies also occur, from acid to basic in compositions. A Permo-Mesozoic meta-sedimentary cover also crops out within the Margna unit (Figs. 1a and b). The whole association of pre-Permian basement, late Variscan intrusive and Permo-Mesozoic cover is involved in the Alpine evolution, producing new mineral associations related to the evolving metamorphic conditions and related structures and folds.

The Margna unit is interpreted as part of the distal margin of the Adria plate (Müntener and Hermann, 2001; Froitzheim et al., 1996), together with the adjacent Malenco ultramafite and ophiolite unit, the former, the Malenco ultramafite, being interpreted as part of a subcontinental mantle exhumed during the Permian extensional evolution and leading to the spreading of the Tethys ocean (*e.g.* Montrasio and Trommsdorff, 1983). The Margna unit records a pre-Alpine high-temperature, intermediate- to low-pressure evolution, likely related to the mentioned extensional tectonic. The thermo-barometrical evolution shows a Permian-Triassic decrease in pressure from 1 to 0.69 GPa associated with a temperature decrease from 760 to 600 °C (Müntener and Hermann, 2001). After these stages a thick Mesozoic sedimentary cover was deposited over the basement rock (Trommsdorff et al., 2005). Afterwards, these units underwent an Alpine deformational and metamorphic stage, started during the Cretaceous (Spalla et al., 1996; Deutsch, 1983; Villa et al., 2000) and characterized by both diffuse and localized plastic and brittle deformation (Montrasio and Trommsdorff, 1983; Bissig and Hermann, 1999). Thermobarometric estimates of the Malenco and Margna units describe an Alpine evolution that reached T = 450–600 °C and P = 0.5–0.8 GPa (Bissig and Hermann, 1999); moreover, mesostructural correlation shows that the Margna and Malenco also share a common deformational evolution during alpine time (Bissig and Hermann, 1999). These observations lead to the interpretation that the Margna and Malenco units were coupled during a relatively shallow burial evolution during the Alpine subduction (Hermann et al., 1997; Montrasio and Trommsdorff, 1983; Müntener and Hermann, 2001). The pre-Alpine tectonometamorphic evolution produced the lithological associations characteristic of the Margna unit, constituted by high-grade sillimanite-bearing gneisses, garnet-bearing amphibolites and olivine-bearing marbles (Fig. 1a, Bedogné et al., 1993; Trommsdorff et al., 2005).

The studied samples were collected within the olivine-bearing marbles and serpentine-rich veins at Pizzo Tremogge (Figs. 1b and c) in the Margna unit. Several samples were collected and divided into four groups: S1, S2, S3 and S4 on the basis of their lithological and structural features.

3. Analytical methods

3.1. Whole rock mineralogical and textural characterization – X-ray powder diffraction (XRPD) and petrographic analyses

The serpentine and its bearing rocks were investigated by petrographic and X-ray powder diffraction (XRPD) analyses. In particular, the mineralogical assemblage was defined by means of XRPD analysis. The samples have been back-loaded on a flat sample-holder and measured by a θ-2θ Bragg Brentano parafocusing PANalytical X'Pert PRO diffractometer, equipped with a multi-channel X'Celerator detector (Cu Kα, with λ = 0.154187 nm). Data were collected in the range 5–80° 2θ with a step size of 0.02° 2θ and a counting time of about 30 s/step. Selected results are shown in Fig. 2. The XRPD qualitative phase analysis of the collected spectra was performed by means of PANalytical X'Pert High Score Plus 2.1.2 software, referring to the ICDD database.

A detailed characterization of the different polymorphs belonging to the serpentine group (*i.e.* lizardite, chrysotile and antigorite) was performed on the investigated samples and, in particular, the < 2 mm fraction of each sample was treated using a McCrone micronizing mill and the resulting powders were then characterized by means of the PANalytical X'Pert PRO diffractometer. Data collection was performed in the range 4–60° 2θ with a step size of 0.002° 2θ and a counting time of about 50 s/step. These experimental conditions allow us to obtain both an accurate position and good statistics on the diffraction peaks, thus permitting a reliable identification of the serpentine minerals occurring in the samples.

In the present text the distinction among the three phases of serpentine (chrysotile, lizardite and antigorite) was performed considering the following reference X-ray powder diffraction patterns of the serpentine minerals in the Powder Diffraction File (PDF) database, as reported in Wicks (2000): chrysotile (10–380), antigorite (7–417) and lizardite (11–386 and 18–779).

3.2. Serpentine characterization – microprobe analysis (WDS)

Quantitative chemical analyses were performed on thin sections, previously studied by optical microscope, using a JEOL JXA-8200 electron microprobe in wavelength-dispersive mode, with an accelerating voltage of 15 kV, a beam current of 5 nA, and counting times of 30 s on peaks and 10 s on backgrounds. The following elements were measured: Si, Al, Ca, Fe, K, Zn, Mn, Mg, Na, Ti, Ni, Cr and Cl. Natural wollastonite (for Si), anorthite (for Al, Ca), fayalite (for Fe), K-feldspar (for K), rhodonite (for Zn and Mn), olivine (for Mg), omphacite (for Na), ilmenite (for Ti), niccolite (for Ni), scapolite (for Cl) and pure Cr (for Cr) have been employed as standards and the raw data were corrected for matrix effects using a conventional ΦρZ routine in the JEOL software package. Representative results are reported in Table 1.

3.3. Serpentine characterization – micro-Raman spectroscopy

Micro-Raman spectroscopic analyses were carried out on the same points of thin sections analyzed by the microprobe.

The analyses were carried out using a Jobin Yvon HR800 LabRam μ-Raman spectrometer equipped with an Olympus BX41 microscope, a HeNe 20 mW laser working at 632.8 nm and a Charge Coupled Device (CCD) air cooled detector. The correct calibration of the instrument was

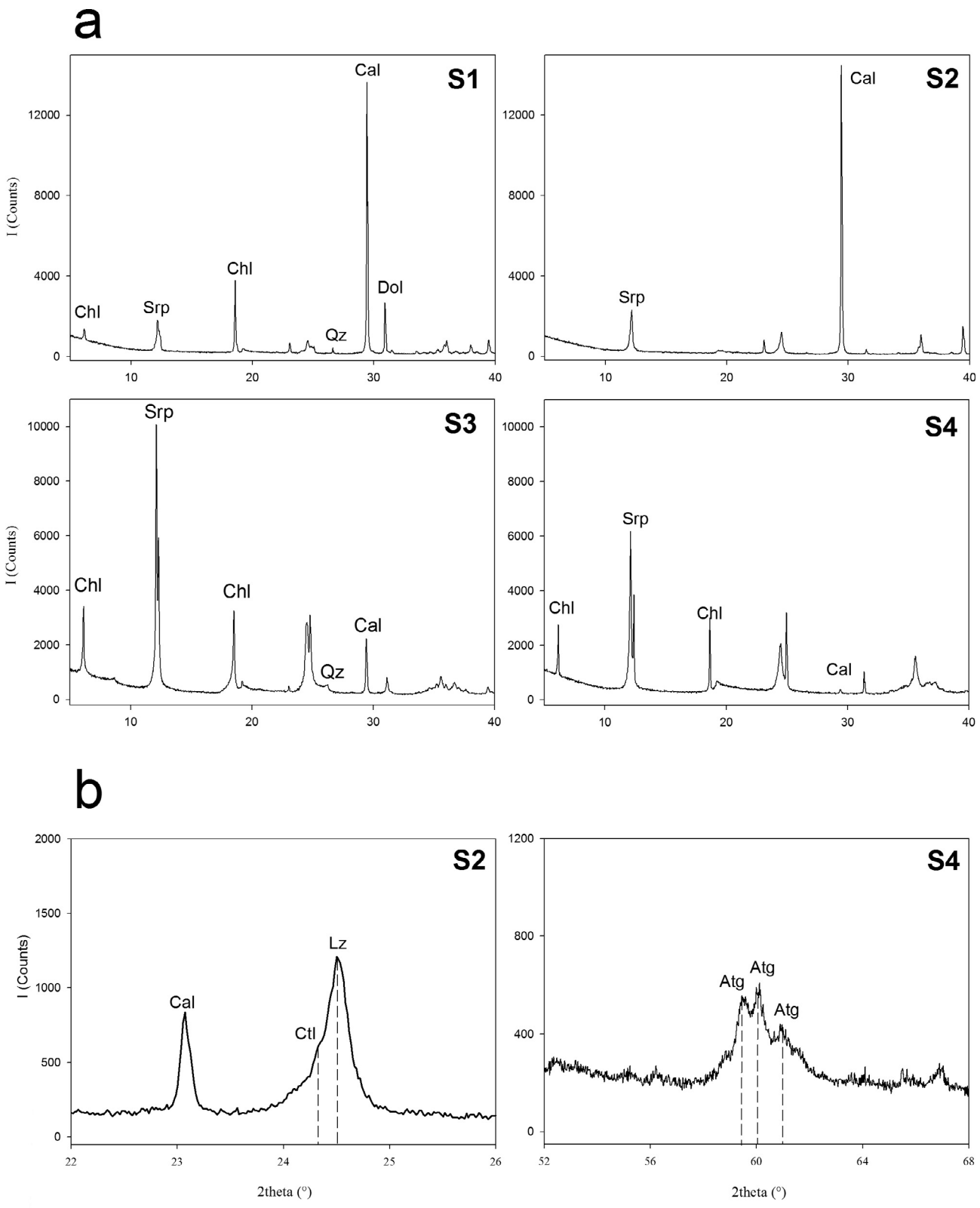

Fig. 2. (a) XRPD patterns of samples S1, S2, S3 and S4; (b) insets of the XRPD of S2 and S4. Mineral abbreviations: Cal: calcite; Chl: chlorite; Qz: quartz; Ol: olivine; Srp: serpentine minerals; Lz: lizardite; Atg: antigorite.

obtained by checking, before every run, position and intensity of the Si band at 520.65 ± 0.05 cm^{-1}. In order to balance signal against noise, at least 50 cycles of 50 s were performed. The spectral region recorded ranged from 1200 cm^{-1} to 100 cm^{-1}, where the vibrational lattice modes of the different minerals lie. The acquired spectra were processed using ORIGIN vers. 6.0 software. When the bands appeared asymmetric, the curve-fitting tool from OPUS software v 4.0 was applied. Band fitting was performed after 9 points FFT smoothing of the

Table 1
Selected microprobe analyses of S1, S2, S3 and S4 samples.

	S1						S2					S3						S4		
wt%	1	2	3	4	5	6	7	8	9	10	11	wt%	12	13	14	15	16	17	18	19
SiO_2	40.43	38.70	39.73	41.03	40.30	29.42	39.03	40.00	40.40	39.82	39.28	SiO_2	41.68	44.85	44.17	42.87	44.84	41.93	43.29	43.30
TiO_2	0.14	0.18	0.15	0.13	0.13	bdl	0.14	0.13	0.13	0.18	0.17	TiO_2	0.04	0.05	0.03	0.06	0.06	0.11	0.09	bdl
Al_2O_3	2.35	2.19	2.93	2.01	2.29	21.58	3.03	3.13	3.01	3.17	3.08	Al_2O_3	0.86	0.65	1.77	2.61	0.81	0.55	0.72	0.20
Cr_2O_3	0.01	0.02	bdl	bdl	bdl	0.08	bdl	bdl	bdl	0.05	bdl	Cr_2O_3	0.05	0.02	0.03	0.03	bdl	bdl	0.05	0.03
FeO_{tot}	3.25	3.39	3.93	3.54	3.83	1.37	2.79	3.16	3.19	3.45	3.07	FeO_{tot}	1.05	0.82	1.40	1.17	0.99	1.71	1.45	1.41
NiO	0.01	0.03	bdl	bdl	0.01	0.04	0.02	bdl	0.04	bdl	bdl	NiO	0.01	bdl	0.02	bdl	bdl	0.04	0.03	0.01
MnO	bdl	bdl	bdl	0.02	0.03	bdl	0.01	bdl	0.00	0.01	0.06	MnO	0.01	0.01	0.01	0.05	0.05	0.01	0.02	0.04
MgO	38.28	38.98	38.54	39.39	38.92	32.04	38.78	38.58	37.55	37.87	38.14	MgO	39.73	38.53	37.92	37.83	38.46	41.13	40.73	40.77
CaO	0.48	0.04	0.07	0.01	0.03	0.08	0.02	0.02	bdl	0.03	0.02	CaO	0.05	0.14	0.02	bdl	0.03	0.01	0.03	0.02
Na_2O	bdl	0.01	0.03	bdl	0.02	0.06	bdl	0.02	bdl	bdl	bdl	Na_2O	0.01	0.02	bdl	bdl	0.02	bdl	0.03	bdl
K_2O	0.01	0.01	0.02	bdl	0.02	0.05	0.01	bdl	0.01	bdl	bdl	K_2O	bdl	bdl	bdl	bdl	0.01	bdl	0.01	bdl
Total	84.97	83.57	85.40	86.14	85.60	84.73	83.82	85.04	84.35	84.63	83.82	Total	83.48	85.08	85.37	84.62	85.26	85.49	86.44	85.79
Cations calculated on the basis of 7 anhydreous oxygens						*														
Si	1.944	1.899	1.909	1.947	1.930	2.817	1.900	1.919	1.950	1.921	1.913	Si	2.010	2.104	2.071	2.029	2.100	1.986	2.019	2.035
Ti	0.005	0.007	0.005	0.005	0.005	–	0.005	0.005	0.005	0.007	0.006	Ti	0.001	0.002	0.001	0.002	0.002	0.004	0.003	–
Al^{IV}	0.056	0.101	0.091	0.053	0.070	–	0.100	0.081	0.050	0.079	0.087	Al^{IV}	–	–	–	–	–	0.014	–	–
Al^{VI}	0.078	0.026	0.075	0.059	0.059	–	0.074	0.096	0.121	0.101	0.090	Al^{VI}	0.049	0.036	0.098	0.146	0.045	0.017	–	0.011
Cr	–	0.001	–	–	–	0.006	–	–	–	0.002	–	Cr	0.002	0.001	0.001	0.001	–	–	0.002	0.001
Fe	0.131	0.139	0.158	0.140	0.153	0.110	0.114	0.127	0.129	0.139	0.125	Fe	0.042	0.032	0.055	0.046	0.039	0.068	0.057	0.055
Ni	–	0.001	–	–	–	0.003	0.001	–	0.002	–	–	Ni	–	–	0.001	–	–	0.002	0.001	–
Mn	–	–	–	0.001	0.001	–	–	–	–	–	0.002	Mn	–	–	–	0.002	0.002	0.001	0.001	0.002
Mg	2.745	2.852	2.761	2.787	2.779	4.574	2.814	2.759	2.702	2.724	2.769	Mg	2.857	2.694	2.651	2.669	2.686	2.904	2.832	2.856
Ca	0.025	0.002	0.004	0.001	0.002	0.008	0.001	0.001	–	0.002	0.001	Ca	0.003	0.007	0.001	–	0.001	0.001	0.001	0.001
Na	–	0.001	0.002	–	0.002	0.010	–	0.002	–	–	–	Na	0.001	0.002	–	–	0.002	–	0.002	–
K	–	0.001	0.001	–	0.001	0.007	0.001	–	0.001	–	–	K	–	–	–	–	–	–	0.001	–
WDS	Lz	Lz	Lz	Lz	Lz	Clc	Lz	Lz	Lz	Lz	Lz	WDS	Ctl-Atg	Ctl-Atg	Ctl-Atg	Ctl-Atg	Ctl-Atg	Ctl-Atg	Atg	Atg
Raman	Ctl	Lz-Clc	Ctl-Cal	Ctl	Ctl	Clc	Lz	Ctl	Lz	Lz	Ctl	Raman	Lz-Ctl	Ctl-Atg	Atg	Atg	Atg	Ctl-Atg	Atg	Atg

bdl = below the detection limit (0.01 wt% for all oxides).
* Cations calculated on the basis of 14 anhydreous oxygens.

spectrum, using a Gaussian function and proposing the minimum number of component bands to obtain reproducible results with the minimal residual error.

The identification of the mineral phases responsible for the observed bands was performed on the basis of the Raman spectra acquired after a careful characterization of their mineralogical assemblages and aspects (Rinaudo et al., 2003; Groppo et al., 2006; Musa et al., 2012; Bloise et al., 2014). The studied spectra were compared with the Raman spectra from the Rruff database.

4. Results

The present section will be divided into two different sub-sections: in the first one ("*Whole rock mineralogical and textural characterization*") the results of the petrographic and XRPD analyses will be presented for each sample group separately. The reported observations are focused on the microstructure and mineralogical assemblage of the serpentine and its bearing rocks; these data will help in clarifying their geological evolution. In the second one ("*Serpentine characterization*") the characterization of the different serpentine generations were determined by coupling petrographic study with microprobe analysis and micro-Raman spectroscopy. These results will be fundamental to clarifying the P-T evolution of serpentine minerals in the whole geodynamic framework of the evolution of the Alps.

Fig. 3 describes main mesoscopic lithological and structural features; serpentine-rich marbles occur as decimetre to metre-thick layers within the marbles, amphibolites and paragneisses rock association (Figs. 3a and c). Main mesostructural features are foliation in marbles, amphibolites and paragneisses (S1 and S2 foliations) and serpentine-rich veins. Fig. 3 reports orientations of such structural features as stereographic projections (Fig. 3f).

Marbles are characterized by a penetrative foliation, S2, testified by one to ten centimetres thick layers rich in yellowish serpentine aggregates that occupy rounded 1–5 mm-thick domains (Fig. 3c). The S2 foliation is constantly dipping toward North, of about 45° (Fig. 3f). This orientation is shared also by paragneisses and amphibolites; in particular, amphibolites record an older foliation (S1) that preserve folding with the axial plane parallel to the dominant S2 foliation (Fig. 3e). Serpentine-filled veins (Fig. 3b and d), commonly dip vertical, describe a high angle with respect to the S2 foliation and postdate the same S2 foliation as revealed by the interruption of S2 foliation by serpentine–filled fractures. Serpentine filling fractures is green and course-grained, easily distinguishable from yellow-green serpentine in marbles.

4.1. Whole rock mineralogical and textural characterization

S1 – The S1 samples (Figs. 4a and b) are a granoblastic marbles

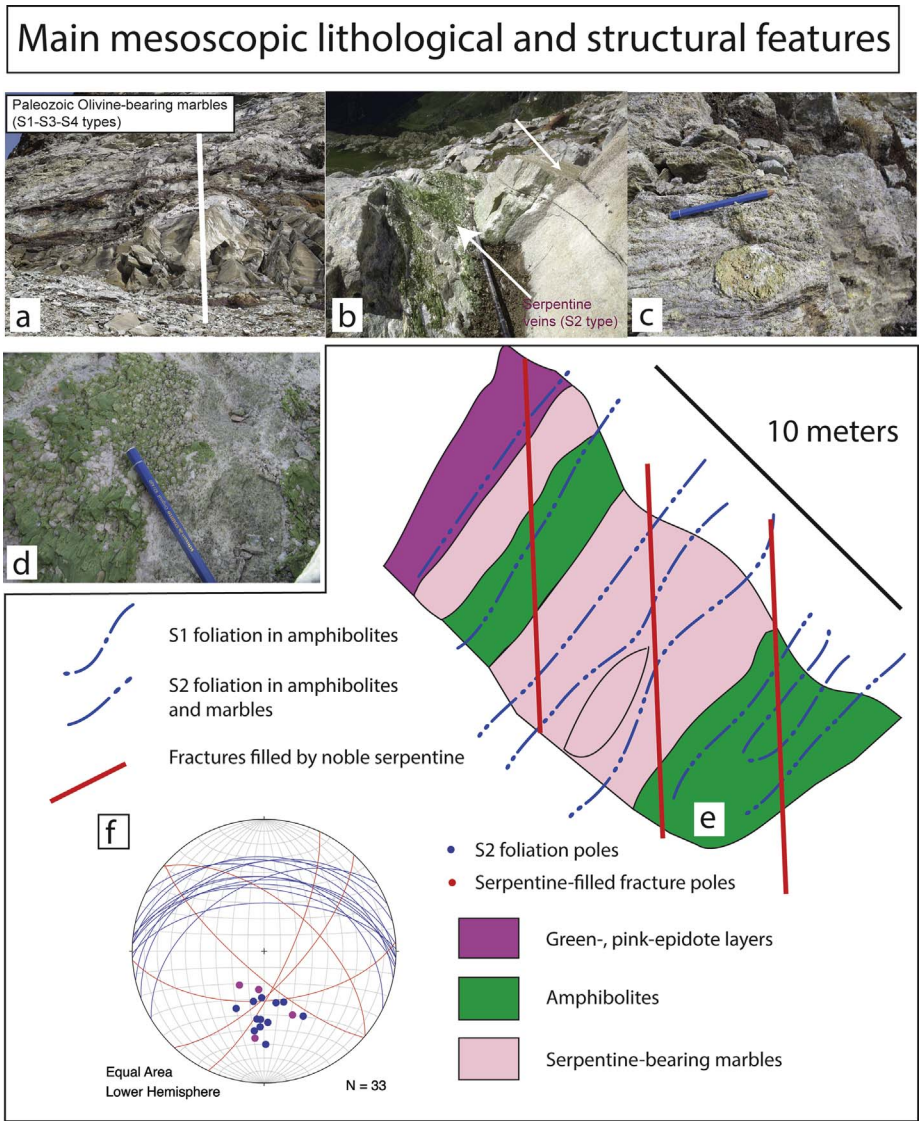

Fig. 3. Main mesoscopic lithological and structural features. (a) particular of serpentine-rich marble layers with the trace of the vertical section of (e); (b) gem-quality green type noble serpentine outcrop found in close association with Palaeozoic marbles; (c) yellow-green type noble serpentine cropping out as pods in Palaeozoic marble layers; (d) particular of (b) of green type noble serpentine along mm-thick fractures; (e) schematic geological cross-section showing geometric relations between lithology and mesostructures with lithological and structural legend; (f) stereographic representation of dominant foliation (S2) and serpentine-filled fractures. (For interpretation of the references to colour in this figure legend, the reader is referred to the web version of this article.)

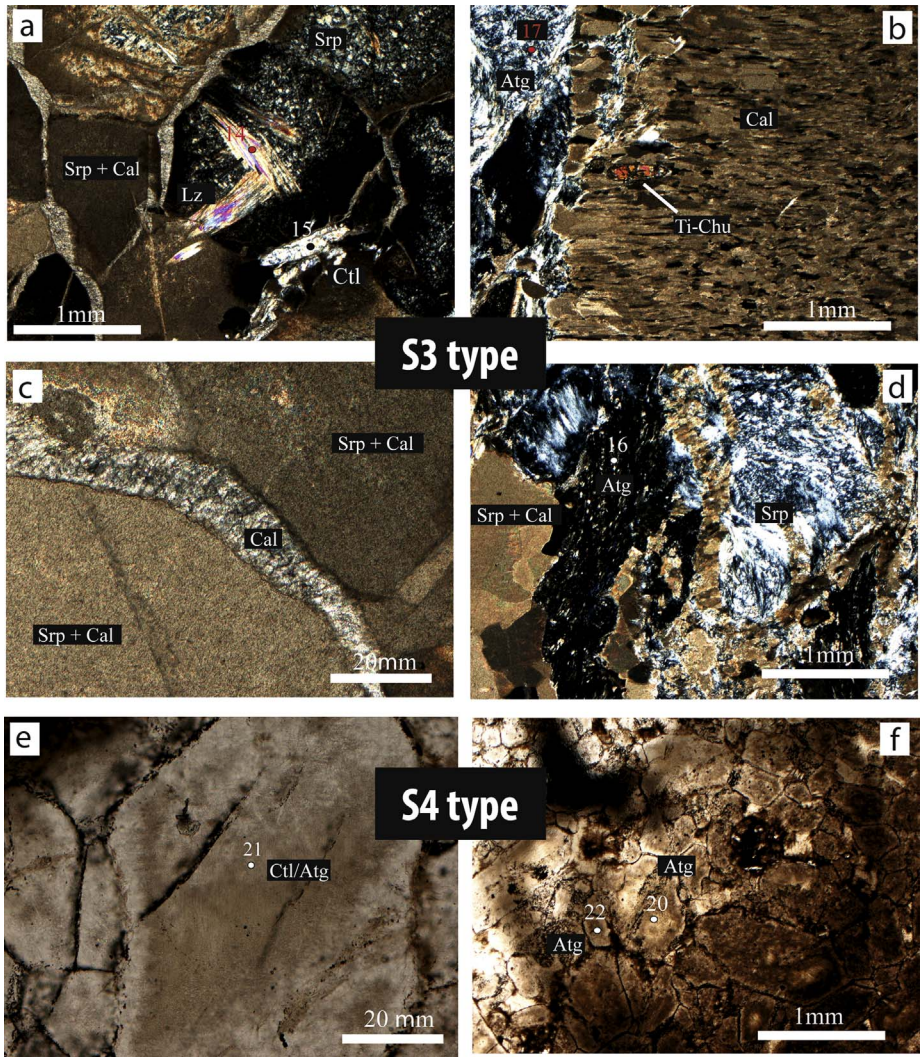

Fig. 4. Photomicrograph of S1 and S2 sample types: (a) Calcite crystals and serpentine aggregates in S1 sample type (2N); (b) S1 sample type showing sub-rounded domains interpreted as earlier olivine domain replaced by serpentine aggregates and brucite (1N); (c) S2 sample type with fibrous calcite veins growing syntaxially (1N); (d) detail of the calcite aggregates in veins that dismember the S2 sample type showing lizardite single crystal (2N); (e) Calcite, chrysotile and quartz veins crosscutting lizardite crystal within S2 sample type (1N); (f) Thin quartz vein post-dating calcite veins and lizardite crystal in S2 sample type (1N). The numbers (from 1 to 10) refer to the point microprobe analysis in Table 1 and Raman referred in the Serpentine – Micro-Raman spectroscopy paragraph.

composed of calcite (60–80%), serpentine (10–30%), chlorite (10–20%), minor brucite and Ti-clinohumite. Calcite grain-size ranges from 100 to 600 μm and the grain boundaries between calcite crystals are commonly straight (Fig. 4a). Serpentine occurs in association with chlorite, describing rounded aggregates which define olivine micro-domains (Fig. 4b). The boundaries between serpentine aggregates are commonly the place of overgrowth by brucite and/or Ti-clinohumite (Fig. 4b). The S1 samples represent a typical olivine-bearing marble (*e.g.* Manzotti and Zucali, 2013) where the olivine domain is substituted by serpentine-rich aggregates.

XRPD analyses confirm the mineralogical assemblage defined by the petrographic observations (Fig. 2a). Furthermore, XRPD also permits the detection of the diffraction peaks for additional dolomite and chlorite and highlights that the dominant serpentine species is lizardite.

S2 – The S2 samples consist of a cm-thick vein hosted in by a S1-type sample (Fig. 1c). Serpentine occurs as centimetre-sized crystals (Fig. 4c). Such single crystals are, in turn, crosscut by two types of structures:

(1) carbonate veins, up to 0.5 mm thick, where the calcite crystals mostly grow syntaxially and show two growing steps: the first one is represented by calcite fibres at high angle with the vein walls and the second one by calcite that is gently bent (Figs. 4c and e). Calcite in veins may also occur as large single crystals (Figs. 4e and f). Microstructural relations suggest that large single crystal calcite veins occur before the syntaxially growth of calcite (Fig. 4e and f).
(2) thin quartz veins (sub-millimetric-thick; Figs. 4e and f) develop at the contact between calcite veins and serpentine crystals but often crosscut them.

The XRPD identifies calcite and serpentine (Fig. 2a), this latter clearly being composed of a mixture of lizardite and chrysotile (Fig. 2b).

S3 and S4 – These samples are characterized by a granoblastic fabric similar to the one observed in S1, where large polygonal calcite domains are associated with rounded aggregates of serpentine (Figs. 5a–f). Fibrous calcite veins occur at the margins of polygonal domains. Differently from the S1 type, calcite single-crystal domains are here replaced by crypto- to microcrystalline aggregates of calcite (Figs. 5a and c) and serpentine. Moreover, some millimetric serpentine lamellae grow over polygonal domains (Fig. 5a). The original grain-size is also easily recognizable, from 100 to 600 μm for calcite large crystals and from 300 to 800 μm for olivine. Extensional veins also occur, filled by fibrous calcite and Ti-clinohumite prismatic crystals (Fig. 5b). Extensional veins crosscut the granoblastic texture and are characterized by syntaxial growth. Calcite aggregates with grain size ranging from 10 to 100 μm mark the grain boundaries of calcite and serpentine aggregates (Figs. 5a and c). Micro-crystalline serpentinitic veins, interdigitated with calcite fibrous veins, cut polygonal domains made of calcite and serpentine aggregates (Fig. 5d).

The XRPD patterns of the two samples are mineralogically very similar and show the coexistence of serpentine minerals with chlorite and

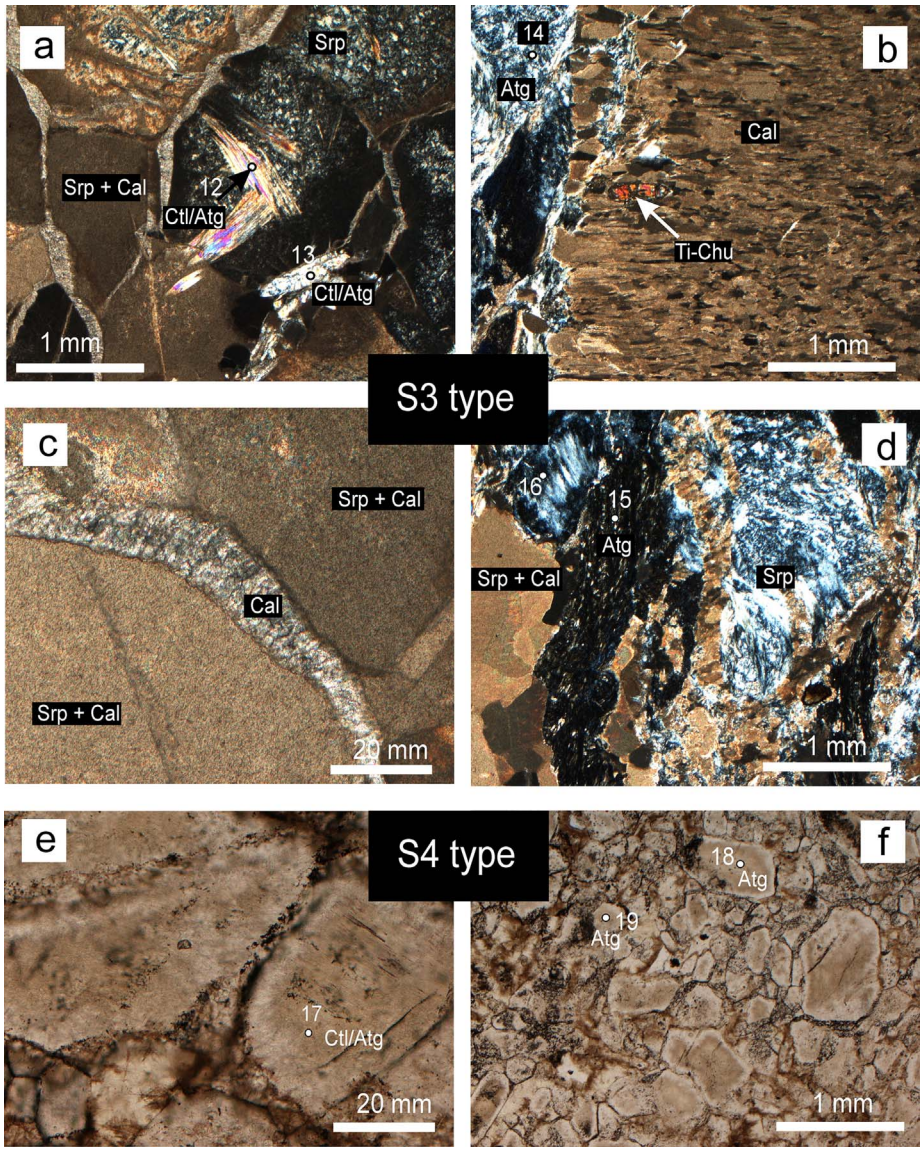

Fig. 5. Photomicrograph of S3-S4 sample types: (a) S3, domains made of fine-grained aggregates of calcite and serpentine with some millimetric chrysotile/antigorite lamellae (2N); (b) S3, extensional vein filled by fibrous calcite and Ti-clinohumite prismatic crystal (2N); (c) S3, fibrous calcite aggregates growing at the boundaries of micro-crypto calcite and serpentine aggregates (2N); (d) S3, serpentinitic veins interdigitate with calcite fibrous veins cutting poligonal domains made of calcite and serpentine aggregates (2N); (e and f) S4 type granoblastic texture largely replaced by aggregates of serpentine, antigorite or chrysotile and calcite.

calcite (Fig. 2a). In Fig. 2b an inset of the diffraction pattern of sample S4 highlights the presence of antigorite as the single pseudo-polymorph belonging to serpentine minerals.

4.2. Serpentine characterization – microprobe analysis (WDS)

Microprobe analyses were performed on the studied thin sections to chemically characterize the serpentine and its mineral assemblage (Table 1) and to select the points for the micro-Raman analysis. Even if microprobe analyses alone are not enough to identify the different serpentine species, a difference between lizardite and antigorite may be highlighted considering the behaviour of Al_2O_3 and FeO_{tot} versus SiO_2.

Following Viti and Mellini (1996, 1997), we considered the extent of cationic substitution: lizardite is always Al and Fe -enriched (Al ranges from 0.07 to 0.2 a.p.f.u., and Fe from 0.12 to 0.17 a.p.f.u., calculated on the basis of 7 anhydrous oxygens) with respect to chrysotile and antigorite (Al ranges from 0.0 to 0.02 a.p.f.u., and Fe from 0 to 0.12 a.p.f.u.). Chrysotile has a wider compositional field but the content of Al_2O_3 never exceeds 2 wt%, independently from the SiO_2 content. In serpentines, chlorine is very low, only in some points resulted above the detection limit, and its values are not reported in Table 1.

The associated phases are chlorite, calcite, brucite and titan-clinohumite, this last with an average composition of $4[Mg_{2.05}Si_{0.95}O_4]$ $[(Mg_{0.5}Ti_{0.4}Fe_{0.07})(OH,F)_2]$, with X_{Ti} ranging from 0.18 to 0.5 and X_{Mg} from 0.31 to 0.73.

As a whole, chemical differences among the samples can be outlined.

In particular:

S1 – The serpentine minerals show an Al content ranging from 0.11 to 0.18 a.p.f.u. whereas Fe varies from 0.10 to 0.26 a.p.f.u., thus classifying the serpentine as lizardite.

Furthermore, we identify the composition of original olivine (inset in Fig. 3b) by performing semi-quantitative areal analysis considering different areas of 500 μm × 500 μm in size. We averaged on 10 areas analyzed using an EDS attached to the electron microscope. The obtained average analysis corresponds to an olivine with a composition of $Fo_{95.6}$ $Fa_{4.4}$.

S2 – In these samples calcite is associated with serpentine, this latter considered as lizardite due to the high content of Al_2O_3, which was always close to 3 wt% (0.17 a.p.f.u.).

S3 and S4 – In these samples serpentine analyses are tentatively identified as chrysotile or antigorite considering the Al and Fe contents, which are lower than in S1 and S2, and the high content of Si, which completely occupies the tetrahedral site.

In Fig. 6 the correlation between the major oxide contents of all samples are reported. Two compositional fields can be distinguished:

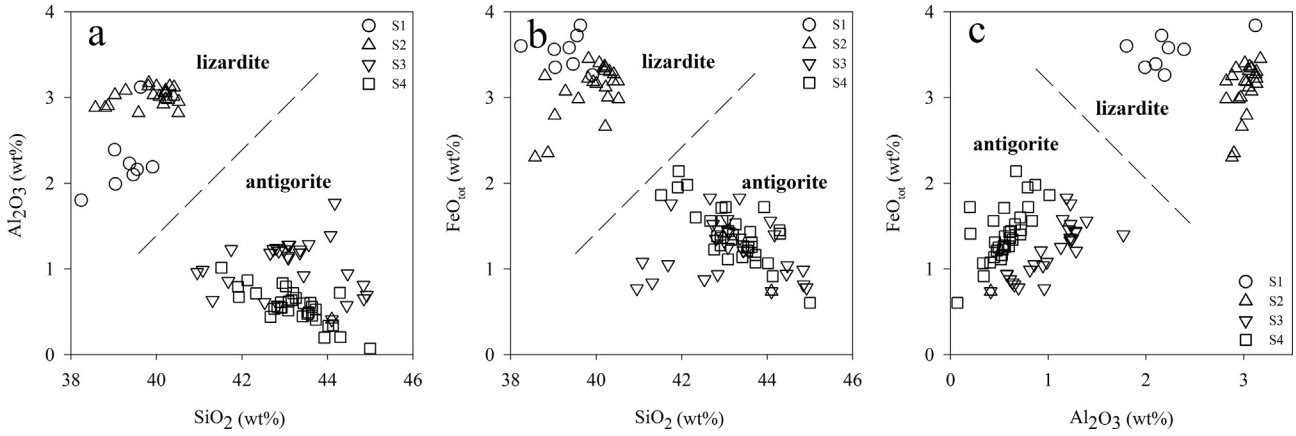

Fig. 6. Scatter plots showing the distribution in serpentine minerals of: (a) Al_2O_3 vs. SiO_2, (b) FeO_{tot} vs. SiO2, and (c) FeO_{tot} vs. Al_2O_3. S1: circles, S2: triangles, S3: upside down triangles, S4: squares.

the first includes S1 and S2 samples and is characterized by enrichment in Al_2O_3, thus reflecting a chemical composition comparable to lizardite. The second contains S3 and S4 samples and displays depletion of Al_2O_3 and the enrichment of SiO_2, both typical features of antigorite.

In general, microprobe analysis allowed us to recognize lizardite and antigorite within the serpentine group while chrysotile is much less easy to discriminate.

4.3. Serpentine characterization – micro-Raman spectroscopy

Several analyses were performed on the different samples and on the same points and areas previously analyzed by WDS microprobe. The serpentine minerals resulted lizardite, antigorite and chrysotile, differently associated.

S1 – In S1 sample the Raman spectra showed an association of lizardite, chrysotile, calcite and clinochlore. In Figs. 7a–d, we report the Raman spectra acquired in points 2, 3 and 6, respectively, and corresponding to the same points in Fig. 4b and Table 1. The detected Raman bands permitted assigning point 2 to an association of lizardite and clinochlore. In particular, the fitting program was applied to the band at 688 cm^{-1}, which appears asymmetric, determining two components lying at 691 and 685 cm^{-1} as shown in Fig. 7b: the first component at 691 cm^{-1} and those at 388 e 238 cm^{-1} in Fig. 7a, may be assigned to lizardite, whereas the second component at 685 cm^{-1} and the bands at 546, 357, 285 and 200 cm^{-1} in Fig. 7a identified clinochlore (Musa et al., 2012). In the spectrum of point 3 (Fig. 7c) two minerals were recognized: chrysotile (bands at 692, 466, 392, 348 and 235 cm^{-1}) and calcite (intense band at 1086 cm^{-1} and a weak band at 712 cm^{-1}, minor component of the chrysotile band at 692 cm^{-1}). All bands of point 6 Raman spectrum (Fig. 7d) were attributed to clinochlore and resulted slightly shifted toward higher wave numbers, similarly to those of clinochlore crystallised at higher pressure (Kleppe et al., 2003).

S2 – Raman spectra of sample S2 resulted in a mixture of lizardite and chrysotile. Two spectra (Figs. 7e and f) were acquired to verify possible differences from the matrix particles, *i.e.*, point 9 in Fig. 4d and the vein mineral composition, *i.e.*, point 10 in Fig. 4d. In both cases lizardite was recognized, with the band occurring near 1095 cm^{-1} peculiar to this variety of serpentine, whereas the other bands lie very close for both lizardite and chrysotile (Rinaudo et al., 2003).

S3 and S4 – In the S3 and S4 samples most analyses reveal a mixture of calcite with the three types of serpentine and confirm the presence of antigorite as already suggested by the XRPD. In the spectrum obtained on the S3 point 12 of Fig. 5a and Table 1 and shown in Fig. 8a, an association of lizardite, calcite and, as a minor component, chrysotile, was deduced. In fact, applying fitting program to the large and asymmetric bands at 692 and 381 cm^{-1}, various band components were recognized: the band at 692 cm^{-1} results composed by three bands, at 711, 694 and 692 cm^{-1} (Fig. 8b) while the band at 381 cm^{-1} shows the presence of a weak component at 391 cm^{-1} (Fig. 8c). This means that the analyzed point is constituted by calcite (bands at 1086, 711 and 284 cm^{-1}), lizardite (bands at 692, 525, 382, 347 and 231 cm^{-1}) and chrysotile (bands at 694, 463, 391 cm^{-1}). The two spectra (Figs. 8d and e) corresponding to S3 points 13 and 14 in Fig. 5a, b and Table 1, were attributed to chrysotile (bands at 693, 464, 391, 348 and 235 cm^{-1}) and antigorite (bands at 1044, 684, 526, 463, 380 and 231 cm^{-1}), respectively (Rinaudo et al., 2003; Groppo et al., 2006). The Raman spectra recorded on S4 sample show the occurrence of antigorite or the association of antigorite and chrysotile. In Fig. 8f an example of the antigorite spectrum corresponding to point 18 in Fig. 5f and Table 1 is reported.

5. Discussion

5.1. Evolutionary stages

On the basis of the micro-scale observations described in the above whole rock characterization sub-section and here interpreted using microstructural criteria (*e.g.* Passchier and Trouw, 1995; Vernon, 2004), we recognized and described three main stages of the rock evolution. The relative chronology between them has been inferred by using geometrical criteria of superposition between mineral phases and structures. We also ascribed to each stage the correct mineral association and composition on the basis of microstructural features as grain boundaries geometry and intra-crystalline deformation (Spalla and Zucali, 2004). Data regarding mineralogy (XRPD), phase chemistry (WDS + EDS) and structure (micro-Raman) have been used to correctly attribute phase association to separate stages. We thus reconstruct a likely relative chronology between microstructures, mineral phases and chemical compositions (Fig. 9).

Stage 1 is represented by the granoblastic texture of calcite and olivine; this is the oldest stage recorded and it is characterized by straight grain boundaries between olivine micro-domains and calcite, suggesting a stable assemblage:

Calcite + Forsterite-rich olivine.

The composition of the olivine has been inferred by areal analysis performed at SEM-EDS on selected microdomains (Fig. 4b) while carbonates have constrained by XRPD, WDS and micro-Raman approaches.

Stage 2 of evolution is marked by the substitution of forsterite-olivine by lizardite (LZ) and chrysotile (CTL) serpentine in fine aggregates ± brucite, following the reactions:

Forsterite + aqueous silica → LZ/CTL-serpentine

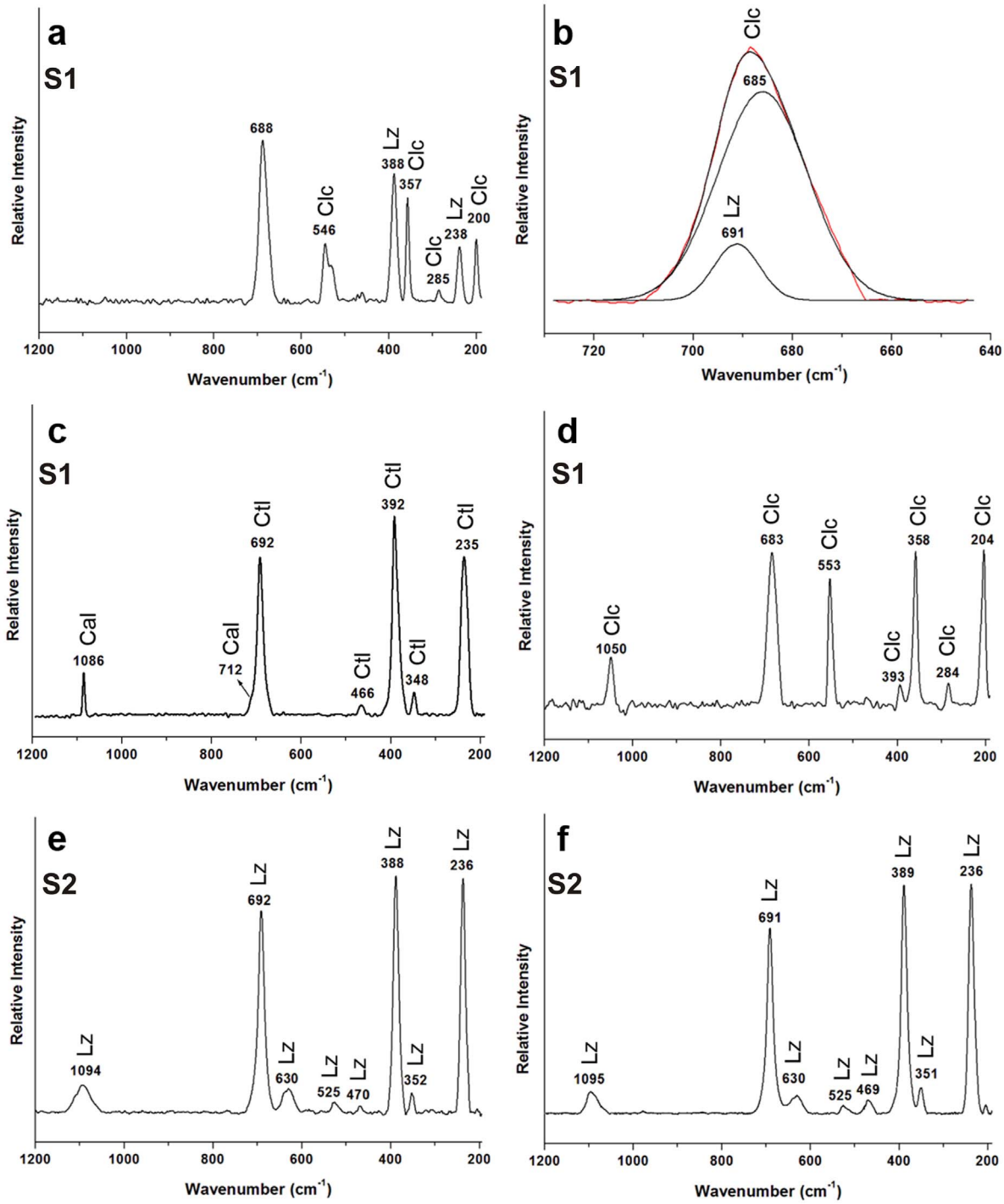

Fig. 7. Micro-Raman spectra of S1 and S2 samples. (a, b) S1: point 2 and deconvolution of 688 cm^{-1} band, Lz-Clc; (c) S1: point 3, Ctl-Cal; (d) S1: point 6, Clc; (e) S2: point 11, Lz; (f) S2: point 12, Lz.

$$3Mg_2SiO_4 + SiO_2 + 4H_2O \rightarrow 2Mg_3Si_2O_5(OH)_4 \quad (1)$$

Forsterite + water → LZ/CTL-serpentine + brucite

$$2Mg_2SiO_4 + 3H_2O \rightarrow Mg_3Si_2O_5(OH)_4 + Mg(OH)_2 \quad (2)$$

The occurrence of lizardite/chrysotile, brucite and serpentine fine-grained aggregates replacing metamorphic olivine clearly requires the income of fluids, hypothesis also supported by the presence of mm-thick veins of lizardite/chrysotile crosscutting the granoblastic fabric of the marble (Figs. 4, 8 and 9).

Stage 3 is associated with fine-grained **antigorite** serpentine that partly replaces lizardite in ex-olivine domains and calcite in granoblastic calcite (Figs. 3 and 5):

LZ/CTL-serp → ATG-serp

These transformations occur synchronously with the development

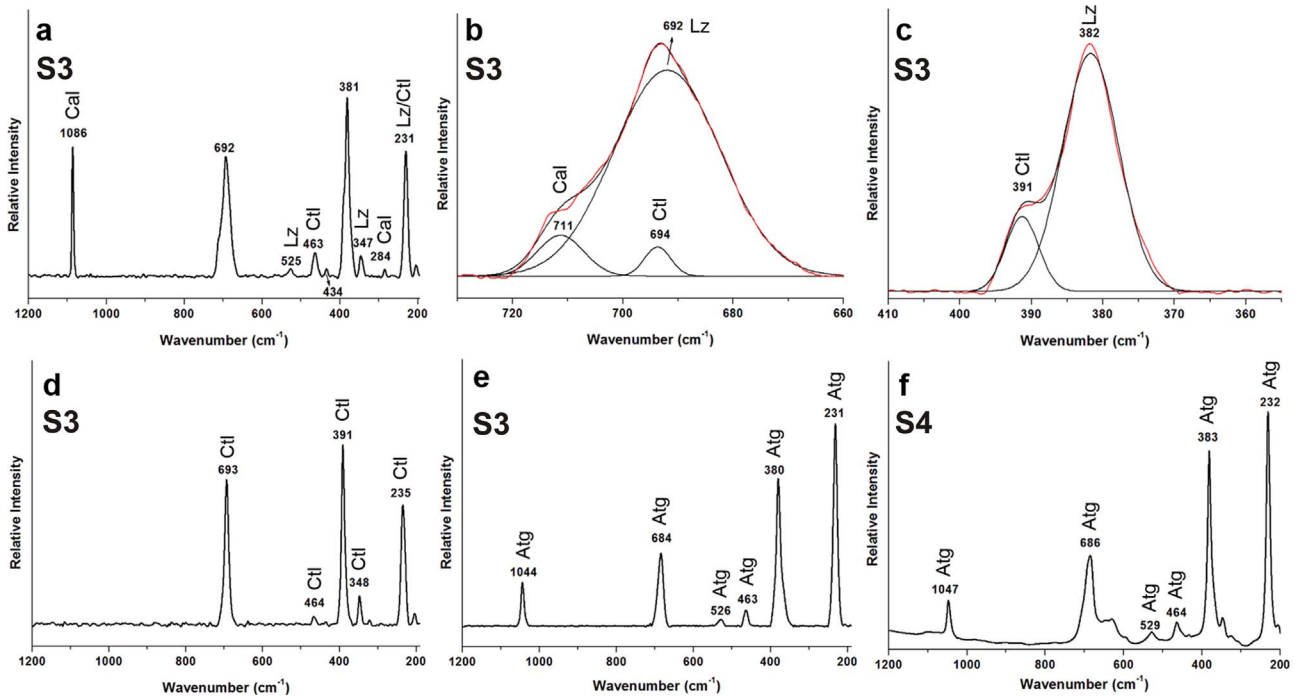

Fig. 8. Micro-Raman spectra of S3 and S4 samples. (a, b and c) S3: point 12 and deconvolutions of 692 and 381 cm^{-1} bands, Lz-Cal-Ctl; (d) S3: point 13, Ctl; (e) S3: point 14, Atg; (f) S4: point 18, Atg.

	STAGE 1	STAGE 2	STAGE 3
Microstructures	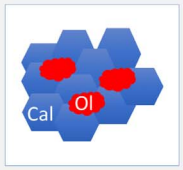 *Figs. 4a-b & 5a-f*	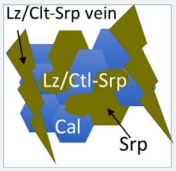 *Figs. 4 & 5*	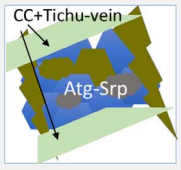 *Figs. 4 & 5*
XRPD	Calcite *Fig. 2*	Calcite + Lz-Srp (ex-olivine) Lz-Srp + Calcite + Qtz (veins)	Calcite + Atg-Srp (ex-olivine and calcite) *Fig. 2*
WDS+EDS (EPMA)	Calcite + Olivine *Fig. 4 + Tab. 1*	Lz/Ctl-Srp in ex-olivine Lz-Srp in veins *Fig. 6 – Tab. 1*	Atg-Srp (ex-olivine and calcite) Calcite + Ti-clinohumite veins Fig. 5
RAMAN	Calcite *Fig. 7 – Tab. 1*	Calcite + Lz/Ctl-Srp + Clc in ex-olivine Lz/Ctl-Srp in veins *Fig. 7 – Tab. 1*	Atg-Srp (ex-olivine and calcite) *Fig. 7 – Tab. 1*

Fig. 9. Schematic representation of the microstructural evolution with related XRPD, WDS-EMPA and RAMAN features. References to specific figures and table are also shown.

of calcite + Ti-clinohumite extensional veins (Fig. 5b), the recrystallization of calcite large grains into fine-grained aggregates of calcite and with calcite rims developing around calcite and olivine domains belonging to stage 1 (Figs. 9 and 10). These microstructures clearly record the transition from lizardite to antigorite, occurring within the stability field of Ti-clinohumite + calcite. Antigorite and calcite + antigorite association in meta-ophicarbonates is documented to be stable at T < 500 °C (Connolly and Trommsdorff, 1991; Schwartz et al., 2013). In addition, Ti-clinohumite in association with calcite and dolomite in olivine/antigorite-saturated metacarbonates is also referred to high-pressure conditions (*e.g.*, Trommsdorff and Evans, 1980; Scambelluri et al., 1997, 2004; Groppo and Compagnoni, 2007; Proyer et al., 2014).

5.2. Geodynamic context of noble serpentine formation

Two sources of "*noble serpentine*" have been reconstructed: i) a green-yellow serpentine type, fine-grained aggregates, occurring in ex-olivine domains during **Stage 2** and **Stage 3**, and ii) a green type, large single crystals, occurring as veins in **Stage 2** (Figs. 1 and 3).

The two occurrences differ not only for their colours and structural features but also for their minero-chemical characters (Fig. 9). In fact, the green-yellow "*noble serpentine*" type may have both lizardite/chrysotile composition, when occurring during **Stage 2**, or antigorite composition during **Stage 3**. The green noble serpentine type has lizardite/chrysotile composition and only occur during **Stage 2**.

Moreover, the green-yellow "*noble serpentine*" type is closely related to olivine-bearing marbles as source rocks and consequently, the presence of olivine-bearing marble is mandatory. The occurrence of olivine-bearing marbles is widely recorded as metamorphic product in continental basement rocks (e.g. Spear, 1993), in association with high-temperature metapelites, locally migmatitic, and metabasites. This association has been described in various settings world-wide but it is also present in the pre-Alpine basement of the Alps (*e.g.* Spalla et al., 2014). This association is also typical in the Margna unit (Figs. 1 and 3) and in the corresponding continental units of the alpine belt (*e.g.* Southern Alps: Diorito-Kinzigitica; Austroalpine: Valpelline Series, Languard-Campo; Helvetic: Argentera Massif). High temperature – intermediate pressure metamorphic conditions have been estimated for this evolution in the Margna unit (Müntener and Hermann, 2001), likely

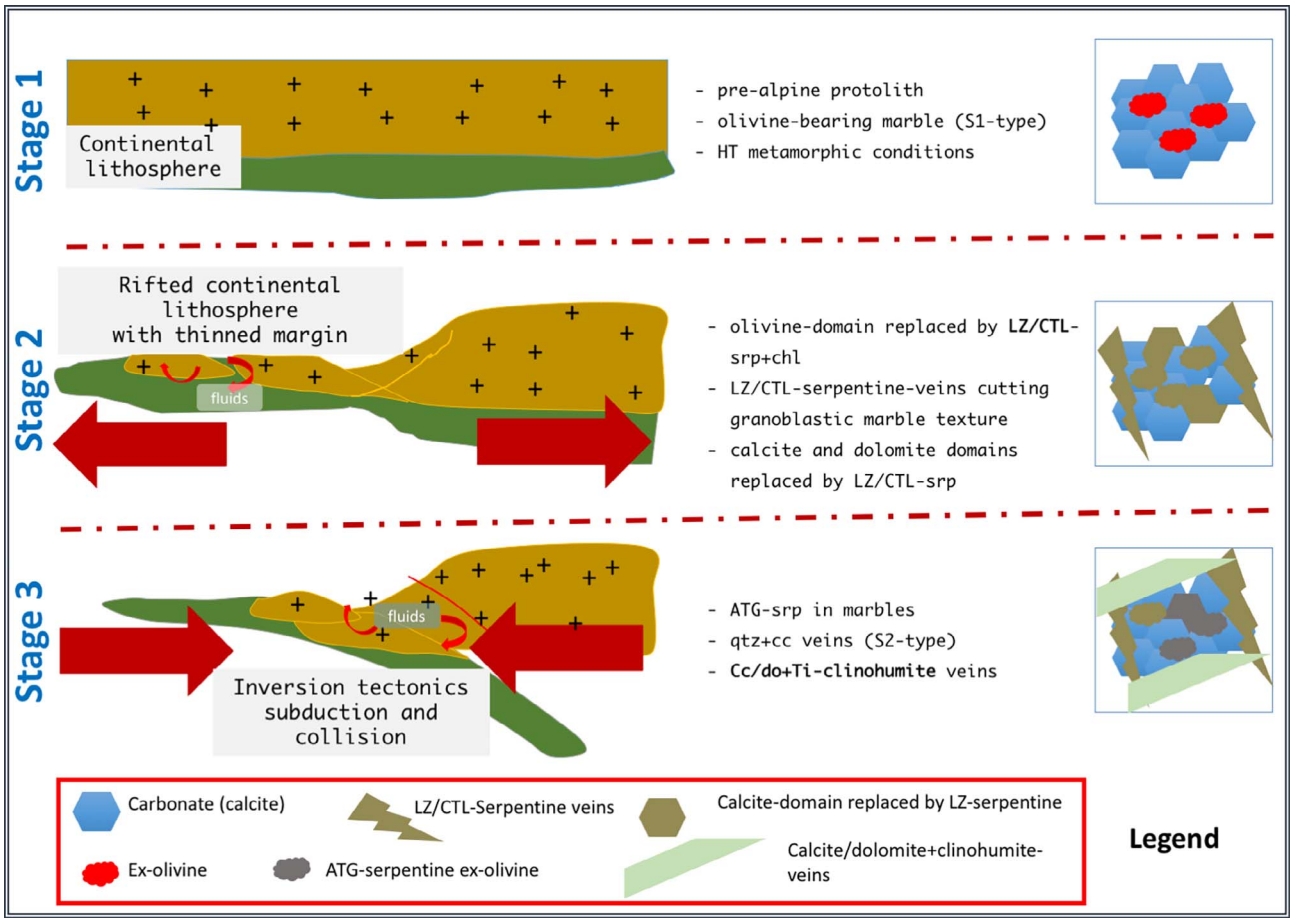

Fig. 10. Evolutionary model for the serpentine-rich deposits and associated Palaeozoic continental lithosphere. Stage 1: forsterite-rich olivine is stable in association with calcite in marbles as part of a stable Palaeozoic crust; Stage 2: olivine (and partially calcite) pseudomorphosed by lizardite during the onset of the extensional tectonics leading to the juxtaposition of serpentinized mantle and continental crust. Lizardite occurs also within vein suggesting fluid circulation; Stage 3: fine-grained antigorite partly replaces lizardite in ex-olivine domains and calcite in granoblastic domains during the alpine convergent tectonics; new veins of calcite and antigorite also occur, suggesting fluid circulation.

associated with the high thermal regime due to the Carboniferous to Permian post-collisional transtensional tectonics (Müntener and Hermann, 2001). We tentatively attribute this stage to a pre-Permian/Triassic basement setting (Fig. 9), related to the Variscan evolution (Schuster et al., 2001; Raumer and Neubauer, 1993).

As described, a **pre-requisite** for the development of "*noble serpentine*" deposit is the presence of a high-temperature migmatitic continental crust, where stable olivine-bearing association in carbonate metasediments could develop (Figs. 9 and 10).

Following this pre-requisite, an income of fluids is also mandatory to efficiently activate the reactions (1) and (2) at metamorphic conditions where lizardite is stable. Specifically, the presence of lizardite (*e.g.* stage 2) is a common finding in the oceanic environment and it is associated with Mg-rich ocean floor type metamorphism (Mével, 2003); moreover, chrysotile and lizardite are generally related to low-pressure conditions more than high pressure – low temperature (Schwartz et al., 2013). The formation of lizardite/chrysotile serpentine during our stage 2 may be ascribed to these conditions.

Olivine-bearing marbles presently close to large bodies of peridotite/serpentinite constituting the Forno-Malenco units (Fig. 1) support these considerations. The juxtaposition of these two rocks likely occurred during the mesozoic extensional evolution of the continental crust (i.e. Margna unit), close to the oceanic transition, as inferred by Bissig and Hermann (1999) for this region. If we agree with their interpretation, continental basement rocks, olivine-bearing marbles included, were close to a source of Mg-rich fluids, at relatively low temperature, as needed to produce chrysotile/lizardite serpentine aggregates.

Moreover, green coloured "*noble serpentine*" type, developed during **Stage 2**, is characterized by lizardite/chrysotile composition (Fig. 9) and also developed along serpentine-rich veins, strongly supporting the presence of Mg-rich fluids channelled within brittle fracture systems, again likely sourcing from the bodies of peridotite/serpentinite of the Forno-Malenco units (Fig. 1), now lying close to the Margna unit.

Conversely, **Stage 3** is also associated with the formation of green-yellow noble serpentine type deposits but with antigorite composition (Fig. 9). Antigorite is associated with Ti-clinohumite, localized in veins and, according to Schwartz et al. (2013), is stable only at low-temperature and relatively high-pressure conditions, contrasting with those inferred for **Stage 2**. Though no geochronological data are available for this evolutionary stage, the attribution to the alpine convergence stage is the only option, up to now, since it justifies baric and thermal conditions, deformation and the presence of fluids (Fig. 9). The alpine deformation is here described as multiphase deformation from a pervasive folding, associated with epidote-amphibolite facies metamorphic conditions (Bissig and Hermann, 1999; Montrasio and Trommsdorff, 2004), to a large scale folding and late thrusting, under greenschist facies conditions.

The detailed reconstruction presented in this work clearly suggests a strong control on the development of "*noble serpentine*" deposits of the tectonic setting, that can range from extensional to convergent. Previous works were mainly focused on mineral composition of "*noble serpentine*" and only few of them linked the formation of "*noble serpentine*" deposits to specific geodynamic settings; Posukhova et al. (2012, 2013) studied several serpentinites from Urals Palaeozoic subduction-collision chain. They found serpentine compositions from

antigorite to lizardite and chrysotile and interpreted these differences as due to distinct tectonic processes though no further insights are proposed. However, it is worth noting that noble yellow-green serpentine, with prevailing antigorite composition, was found in similar polymetamorphic metacarbonates (Posukhova et al., 2012, 2013).

6. Conclusions

An investigation of serpentine included in Palaeozoic olivine-bearing marbles occurring in the Margna unit (Central Austroalpine domain) and sampled at Pizzo Tremogge (Val Malenco, Italy) was performed by means of optical microscopy, X-ray powder diffraction, EMPA and micro-Raman spectroscopy.

The sample microstructure highlighted through petrographic observations coupled with the phase assemblage detected by XRPD, permits a reconstruction of the geological evolution of the "*noble serpentine*" occurring in the serpentine-pure veins and in Palaeozoic olivine-bearing marbles.

On the other hand, the serpentine chemical compositions, revealed through EMPA, XRPD and Raman analyses, allow to infer and clarify the geological evolution of serpentine within the whole geodynamic framework of the pre-alpine and alpine evolution of the Alps.

It turns out that "*noble serpentine*" occurs in olivine-bearing marbles thanks to an income of fluids interacting with host rocks both during extensional tectonics, also associated with the development of pure noble serpentine veins, and during convergent/subduction tectonics where fluids are frequent.

The two types of "*noble serpentine*" origins have been quantified and fully characterized.

Acknowledgements

This research did not receive any specific grant from funding agencies in the public, commercial, or not-for-profit sectors. We greatly acknowledge Mr P. Nana for its help in the field work, and two anonymous reviewers for their comments and suggestions which remarkably improved the quality of the manuscript.

Appendix A. Supplementary data

Supplementary data associated with this article can be found, in the online version, at http://dx.doi.org/10.1016/j.oregeorev.2017.11.020. These data include Google maps of the most important areas described in this article.

References

Adamo, I., Bocchio, R., Diella, V., Pavese, A., Vignola, P., Prosperi, L., Palanza, V., 2009. Demantoid garnet from Val Malenco, Italy: review and update. Gems Gemol. 45, 280–287.

Adamo, I., Diella, V., Bocchio, R., Marinoni, N., Mainardi, M., Fontana, E., Rinaudo, C., 2014. "Noble serpentine": a case study from Val Malenco, Central Alps, Italy. Plinius 40, 329.

Adamo, I., Diella, V., Bocchio, R., Rinaudo, C., Marinoni, N., 2016. Gem-quality serpentine from Valmalenco, Central Alps, Italy. Gems Gemol. 52, 38–49.

Andreani, M., Baronnet, A., Boullier, A., Gratier, J., 2004. A microstructural study of a "crack-seal" type serpentine veins using SE and TEM techniques. Eur. J. Mineral. 16, 585–595.

Andreani, M., Grauby, O., Baronnet, A., Monoz, M., 2008. Occurrence, composition and growth of polyhedral serpentine. Eur. J. Mineral. 20, 159–171.

Bedogné, F., Montrasio, A., Sciesa, E., 1993. I minerali della provincia di Sondrio, Valmalenco. Bettini, Sondrio-Italy, pp. 275.

Benetti, F., 1984. I minerali del pizzo Tremogge in val Malenco. Benetti, Sondrio-Italy, pp. 70.

Bissig, T., Hermann, J., 1999. From pre-Alpine extension to Alpine convergence: the example of the southwestern margin of the Margna nappe (Val Malenco, N-Italy). Schweiz. Mineral. Petrogr. Mitt. 79, 363–380.

Bloise, A., Critelli, T., Catalano, M., Apollaro, C., Miriello, D., Croce, A., Barrese, E., Liberi, F., Piluso, E., Rinaudo, C., Belluso, E., 2014. Asbestos and other fibrous minerals contained in the serpentinites of the Gimigliano-Mount Reventino Unit (Calabria, S-Italy). Environ. Earth Sci. 71, 3773–3786.

Bromiley, G.D., Pawley, A.R., 2003. The stability of antigorite in the systems MgO-SiO_2-H2O (MSH) and MgO-Al_2O_3-SiO_2-H_2O (MASH): the effects of Al^{3+} substitution on high-pressure stability. Am. Mineral. 88, 99–108.

Connolly, J.A.D., Trommsdorff, V., 1991. Petrogenetic grids for metacarbonate rocks: pressure-temperature phase-diagram projection for mixed-volatile systems. Contrib. Miner. Petrol. 108, 93–105.

Deutsch, A., 1983. Datierungen an Alkaliamphibolen und Stilpnomelan aus der suedlichen Platta-Decke (Graubunden). Eclogae Geol. Helv. 76, 295–308.

Dodony, I., Posfai, M., Buseck, P.R., 2002. Revised structure models for antigorite: an HRTEM study. Am. Mineral. 87, 1443–1457.

Evans, B.W., 2004. The serpentinite multisystem revisited: chrysotile is metastable. Int. Geol. Rev. 46, 479–506.

Evans, B.W., Hattori, K., Barronet, A., 2013. Serpentinite: what, why, where? Elements 9, 99–106.

Froitzheim, N., Schmid, S.M., Frey, M., 1996. Mesozoic paleogeography and the timing of eclogite-facies metamorphism in the Alps: a working hypothesis. Eclogae Geol. Helv. 110, 81–110.

Groppo, C., Rinaudo, C., Cairo, S., Gastaldi, D., Compagnoni, R., 2006. Micro-Raman spectroscopy for a quick and reliable identification of serpentine minerals from ultramafics. Eur. J. Mineral. 18, 319–329.

Groppo, C., Compagnoni, R., 2007. Metamorphic veins from the serpentinites of the Piemonte Zone, Western Alps, Italy: a review. Period. Mineral. 76, 127–153.

Hermann, J., Müntener, O., Trommsdorff, V., Hansmann, W., Piccardo, G.B., 1997. Fossil crust-to-mantle transition, Val Malenco (Italian Alps). J. Geophys. Res. 102 (B9), 20123–20132.

Hilairet, N., Daniel, I., Reynard, B., 2006. Equation of state of antigorite, stability field of serpentines, and seismicity in subduction zones. Geophys. Res. Lett. 33, L02302.

Kleppe, A.K., Jephcoat, A.P., Welch, M.D., 2003. The effect of pressure upon hydrogen bonding in chlorite: a Raman spectroscopic study of clinochlore to 26.5 GPa. Am. Mineral. 88, 567–573.

Laurora, A., Brigatti, M.F., Malferrari, D., Galli, E., Rossi, A., 2011. The crystal chemistry of lizardite-1T from northern Apennines ophiolites near Modena, Italy. Can. Mineral. 49, 1045–1054.

Manzotti, P., Zucali, M., 2013. The pre-Alpine tectonic history of the Austroalpine continental basement in the Valpelline unit (Western Italian Alps). Geol. Mag. 150, 153–172.

Mével, C., 2003. Serpentinization of abyssal peridotites at mid-ocean ridges. C. R. Geosci. 335, 825–852.

Montrasio, A., Trommsdorff, V., 1983. Guida all'escursione del Massiccio di Val Masino-Bregaglia. Val Malenco occidentale, Sondrio. Memorie della Soc. Geol. Ital. 26, 421–434.

Montrasio, A., Trommsdorff, V., 2004. Carta geologica della Valmalenco, in scala 1:25.000. CNR Quaderni di Geodinamica Alpina e Quaternaria 8, 1–16.

Müntener, O., Hermann, J., 2001. The role of lower crust and continental upper mantle during formation of non-volcanic passive margins: evidence from the Alps. Geol. Soc. Lond. Specl. Publ. 197, 267–288.

Musa, M., Croce, A., Allegrina, M., Rinaudo, C., Belluso, E., Bellis, D., Toffalorio, F., Veronesi, G., 2012. The use of Raman spectroscopy to identify inorganic phases in iatrogenic pathological lesions of patients with malignant pleural mesothelioma. Vib. Spectrosc. 61, 66–71.

Padrón-Navarta, J.A., Sánchez-Vizcaíno, V.L., Hermann, J., Connolly, J.A.D., Garrido, C.J., Gómez-Pugnaire, M.T., Marchesi, C., 2013. Tschermak's substitution in antigorite and consequences for phase relations and water liberation in high-grade serpentinites. Lithos 178, 186–196.

Passchier, C.W., Trouw, R.A.J., 1995. Microtectonics. Springer, Berlin.

Posukhova, T.V., Panasian, L.L., Cherepetskaya, E.B., Sas, I.E., 2012. Mineralogical features and properties of serpentine as indicator of the deep earth subduction processes. J. Earth Sci. Eng. 2, 729–743.

Posukhova, T.V., Panasian, L.L., Sas, I.E., 2013. Serpentinites of the ural: mineralogical features, petrophysical properties and subduction processes. Open J. Geol. 3, 250–261.

Proyer, A., Baziotis, I., Mposkos, E., Rhede, D., 2014. Ti- and Zr-minerals in calcite-dolomite marbles from the ultrahigh-pressure Kimi Complex, Rhodope mountains, Greece: implications for the P-T evolution based on reaction textures, petrogenetic grids, and geothermobarometry. Am. Mineral. 99, 1429–1448.

Raumer, J.F.v., Neubauer, F., 1993. Pre-Mesozoic Geology in the Alps. Springer-Verlag, Berlin Heidelberg, pp. 667. http://dx.doi.org/10.1007/978-3-642-84640-3.

Rinaudo, C., Gastaldi, D., Belluso, E., 2003. Characterization of chrysotile, antigorite and lizardite by FT-Raman spectroscopy. Can. Mineral. 41, 883–890.

Scambelluri, M., Piccardo, G.B., Philippot, P., Robbiano, A., Negretti, L., 1997. High salinity fluid inclusions formed from recycled seawater in deeply subducted alpine serpentinite. Earth Planet. Sci. Lett. 148, 485–499.

Scambelluri, M., Müntener, O., Ottolini, L., Pettke, T.T., Vannucci, R., 2004. The fate of B, Cl and Li in the subducted oceanic mantle and in the antigorite breakdown fluids. Earth Planet. Sci. Lett. 222, 217–234.

Schuster, R., Scharbert, S., Abart, R., Frank, W., 2001. Permo-Triassic extension and related HT/LP metamorphism in the Austroalpine-Southalpine realm. Mitt. Ges. Geol. Bergbaustub Österr. 45, 111–141. http://dx.doi.org/10.1524/9783486730777.ix.

Schwartz, S., Guillot, S., Reynard, B., Lafay, R., Debret, B., Nicollet, C., Lanari, P., Auzende, A.L., 2013. Pressure-temperature estimates of the lizardite/antigorite transition in high pressure serpentinites. Lithos 178, 197–210.

Spalla, M.I., Lardeaux, J.M., Dal Piaz, G.V., Gosso, G., Messiga, B., 1996. Tectonic significance of Alpine eclogites. J. Geodyn. 21, 257–285.

Spalla, M.I., Zucali, M., 2004. Deformation vs. metamorphic re-equilibrium heterogeneities in polymetamorphic rocks; a key to infer quality P-T-d-t path. Period. Mineral. 73, 249–257.

Spalla, M.I., Zanoni, D., Marotta, A.M., Rebay, G., Roda, M., Zucali, M., Gosso, G., 2014. The transition from Variscan collision to continental break-up in the Alps: insights from the comparison between natural data and numerical model predictions. Geol. Soc. Lond. Specl. Publ. 405, 363–400.

Spear, F., 1993. Metamorphic Phase Equilibria and Pressure-temperature-time Paths. Mineralogical Society of America, Washington, D.C.

Trommsdorff, V., Evans, B.W., 1980. Titanian hydroxyl-clinohumite: formation and breakdown in antigorite rocks (Malenco, Italy). Contrib. Miner. Petrol. 72, 229–242.

Trommsdorff, V., Montrasio, A., Hermann, J., Müntener, O., Spillmann, P., Gieré, R., 2005. The geological map of Valmalenco. Schweiz. Mineral. Petrogr. Mitt. 85, 1–13.

Ulmer, P., Trommsdorff, V., 1995. Serpentine stability to mantle depths and subduction-related magmatism. Science 268, 858–861. http://dx.doi.org/10.1126/science.268.5212.858.

Ulmer, P., Trommsdorff, V., 1999. Phase relations of hydrous mantle subducting to 300 km. In: Fei, Y., Bertka, C.M., Mysen, B.O. (Eds.), Mantle Petrology: Field Observations and High Pressure Experimentation. The Geochemical Society, pp. 259–281.

Vernon, R.H., 2004. A Practical Guide to Rock Microstructure. Cambridge University Press, Cambridge, UK.

Villa, I.M., Hermann, J., Muentener, O., Trommsdorff, V., 2000. ^{39}Ar-^{40}Ar dating of multiply zoned amphibole generations (Malenco, Italian Alps). Contrib. Miner. Petrol. 140, 363–381.

Viti, C., Mellini, M., 1996. Vein antigorites from Elba Island, Italy. Eur. J. Mineral. 8, 423–4344.

Viti, C., Mellini, M., 1997. Contrasting chemical compositions in associated lizardite and chrysotile in vein from Elba, Italy. Eur. J. Mineral. 9, 585–596.

Wicks, F.J., 2000. Status of the reference X-ray powder-diffraction patterns for the serpentine minerals in the PDF database-1997. Powder Diffr. 15, 42–50.

Wicks, F.J., O'Hanley, D.S., 1988. Serpentine minerals: structure and petrology. In: Bailey, SW. (Ed.), Hydrous Phyllosilicates (Exclusive of Micas). Reviews in Mineralogy 19. pp. 91–168.

Wunder, B., Schreyer, W., 1997. Antigorite: high-pressure stability in the system $MgOSiO_2H_2O$ (MSH). Lithos 41 (1–3), 213–227.